

## Supporting Information

# High-Entropy Alloys as Catalysts for the CO<sub>2</sub> and CO Reduction Reactions—Part II: Experimental Realization

Subramanian Nellaiappan<sup>†‡</sup>, Nirmal Kumar Katiyar<sup>§‡</sup>, Ritesh Kumar<sup>δ‡</sup>, Arko Parui<sup>δ</sup>, Kirtiman Deo Malviya<sup>Υ</sup>, K. G. Pradeep<sup>‡</sup>, Abhishek K. Singh<sup>δ\*</sup>, Sudhanshu Sharma<sup>†\*</sup>, Chandra Sekhar Tiwary<sup>#\*</sup>, Krishanu Biswas<sup>§\*</sup>

<sup>†</sup>*Department of Chemistry, Indian Institute of Technology Gandhinagar, Gandhinagar - 382355, INDIA; Email: ssharma@iitgn.ac.in*

<sup>§</sup>*Department of Materials Science and Engineering, Indian Institute of Technology Kanpur, Kanpur-208016, INDIA; Email: kbiswas@iitk.ac.in*

<sup>δ</sup>*Materials Research Center, Indian Institute of Science, Bangalore-560012, INDIA; Email: abhishek@iisc.ac.in*

<sup>Υ</sup>*Department of Materials Engineering, Indian Institute of Science, Bangalore-560012, INDIA*

<sup>‡</sup>*Department of Materials Science and Metallurgical Engineering, Indian Institute of Technology Madras, Chennai-600036, INDIA*

<sup>#</sup>*Metallurgical and Materials Engineering, Indian Institute of Technology Kharagpur, Kharagpur-382355, INDIA; Email: Chandra.tiwary@metal.iitkgp.ac.in*

<sup>‡</sup>Authors have contributed equally in this work.

## MATERIALS AND METHODS

The high entropy alloy (HEA) nanoparticles have been prepared using cast cum cryo-milling process. In which, the Au, Ag, Pd, Pt and Cu (99.9 at. % pure, Alfa Aesar, USA) melted under argon environment to synthesize cast HEAs and afterward cast HEA have been milled in cryomill for 6 hours. The detailed synthesis process can be found elsewhere.<sup>1</sup> The cryomilled powder (HEA nanoparticles) has been characterized in order to the crystalline phase, size, chemical homogeneity, composition, and catalyst activity. The X-ray diffraction recorded using Panalytical empyrean ( $\lambda_{\max}=1.54056$  Å), and size of nanoparticles have been estimated using Transmission electron microscope (FEI, Technai G<sup>2</sup>, UT 20 operated at 200

kV). The surface composition has been estimated using X-ray photoelectron spectroscopy (PHI 5000 Versa Prob II, FEI Inc.).

Electrochemical studies were performed using the conventional three-electrode system using CHI408C electrochemical workstation. All solutions were prepared using double-distilled water. The working electrode was made by mixing 100 mg of catalyst, 200  $\mu$ L of 5% Nafion solution (binder) and 300  $\mu$ l of isopropanol. The resulting slurry was deposited on a glassy carbon electrode (GCE) with the geometric area of 0.071 cm<sup>2</sup>. Platinum wire/electrode was used as the counter electrode, and Ag/AgCl electrode was used as the reference electrode. 0.5 M K<sub>2</sub>SO<sub>4</sub> (pH = 7) was used as the supporting electrolyte. The conversion of potential to reversible hydrogen electrode (RHE) was calculated using the following equation:  $E(\text{RHE}) = E(\text{Ag/AgCl}) + (0.196 + 0.059 \text{ pH})$ . For CO<sub>2</sub> electroreduction, the electrolyte was saturated with N<sub>2</sub> or CO<sub>2</sub> (purging for 30 minutes). An air-tight electrochemical cell was used for the gaseous product collection and analysis. For quantification of gaseous products, 1 mL syringe was used to transfer the evolved gases into a gas chromatograph (CIC Baroda). Haysep-A column was used for separation, and a Flame Ionization Detector (FID) is used for detection of carbonaceous products. Thermal Conductivity Detector (TCD) for H<sub>2</sub> detection. Current and faradaic efficiencies were estimated using the following relationships:

$$\text{CE}\% = \frac{i_{\text{CO}_2} - i_{\text{blank}}}{i_{\text{CO}_2}} \times 100 \quad (\text{S1})$$

Here,  $i_{\text{CO}_2}$  is the current measured in the CO<sub>2</sub>-saturated and  $i_{\text{blank}}$  is the current obtained in N<sub>2</sub> saturated 0.5 M K<sub>2</sub>SO<sub>4</sub> electrolyte.

$$\text{FE}\% = \frac{n \times F \times N}{Q} \times 100 \quad (\text{S2})$$

Here,  $n$  is the number of electrons transferred in the faradaic process;  $F$  is Faraday constant;  $N$  is the amount of the generated product in this process;  $Q$  is the total charge passed through the whole reaction.

The Vienna ab-initio simulation (VASP 5.4.1) package<sup>2</sup> was utilized for performing all the first-principles calculations. The all-electron projector augmented wave (PAW) pseudopotentials were used for describing the interactions between electrons and

ions. Perdew-Burke-Ernzerhof (PBE) generalized gradient approximation (GGA) was used for approximating electronic exchange and correlation effects.<sup>3</sup> An energy cut-off of 500 eV was used for selecting the planewaves. All the structures optimization was performed using a conjugate gradient scheme until the energies, and the components of forces reached  $10^{-5}$  eV and  $0.01$  eV  $\text{\AA}^{-1}$ , respectively. A vacuum of  $15$   $\text{\AA}$  was added in the Z-direction to prevent interactions between the periodic images. Brillouin zone was sampled by a  $2 \times 4 \times 1$  Monkhorst-Pack grid for slab calculations. The (111) surfaces of Pt and Cu were generated from the respective optimized bulk structures using Virtual NanoLab version 2016.2. The method of special quasirandom structure (SQS) was utilized for approximating the AuAgPtPdCu HEA, as SQS represent the best periodic approximation to the true disordered state<sup>4</sup>. It was generated from  $5 \times 3 \times 1$  supercell of Pt (111) surface by using Alloy Theoretic Automated Toolkit (ATAT)<sup>5</sup> code. These quasirandom structures are generated in ATAT through a Monte Carlo simulated annealing method using an objective function that perfectly matches the maximum number of correlation functions<sup>5</sup>. Such SQS can mimic the thermodynamic and electronic properties of actual structures to a reasonable extent, as has been exemplified in the earlier reports<sup>6,7</sup>. At first, “corrump” utility is utilized for generating clusters using some guess range of pairs or triplets employed in the cluster expansions. Then SQS structures are generated using “mcsqs” utility, where it tries to minimize the objective function. It may run indefinitely for larger structures such as ours, so the code is prematurely stopped. The file “bestcorr.out” contain the range of pairs of the cluster of the best SQS found so far. This value of range of pair is used in running the “corrump” utility again, and then “mcsqs” utility at last. Three such SQS structures were generated in our case using different range of pairs, and are shown in Fig. S3. DOS for the three configurations of HEA SQS are also shown in Fig. S4, where it is clear that there is not much difference in their electronic properties. The SQS structure shown in Fig. S3(a) is minimum in energy and was utilized for further calculations. To mimic the bulk behavior, the bottom two layers were frozen and only the topmost layer was allowed to relax, out of the total three layers in the Cu (111) and HEA slab.

**Figure S1**

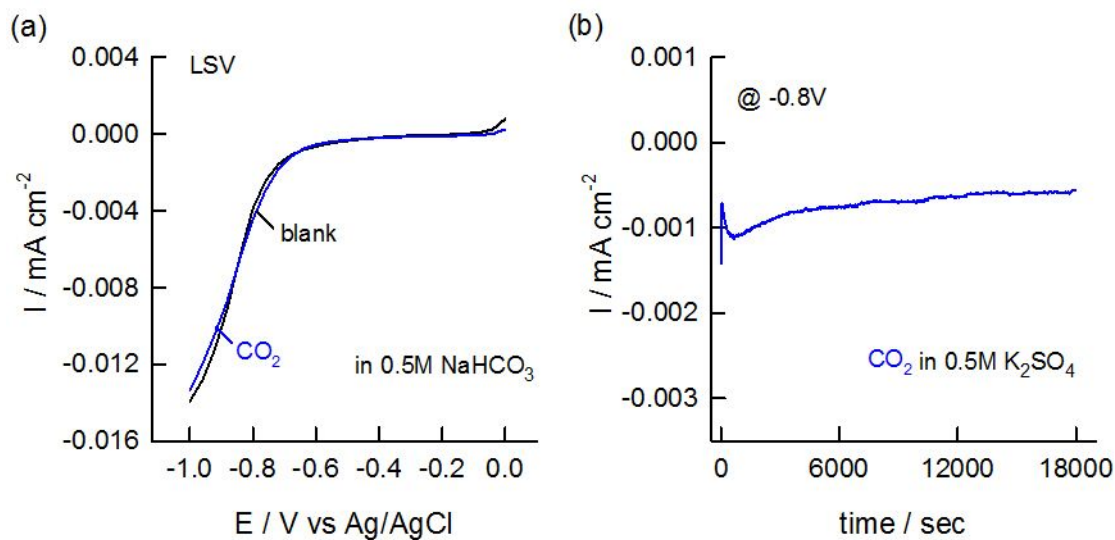


**Figure S1.** Linear sweep voltammetric response of HEA in CO<sub>2</sub> saturated 0.5 M NaHCO<sub>3</sub> electrolyte at 20 mV s<sup>-1</sup> scan rate (a) and long-term stability for CO<sub>2</sub> catalysis on HEA up to 5 hrs in CO<sub>2</sub> bubbling K<sub>2</sub>SO<sub>4</sub> electrolyte solution (b).

**Figure S2**

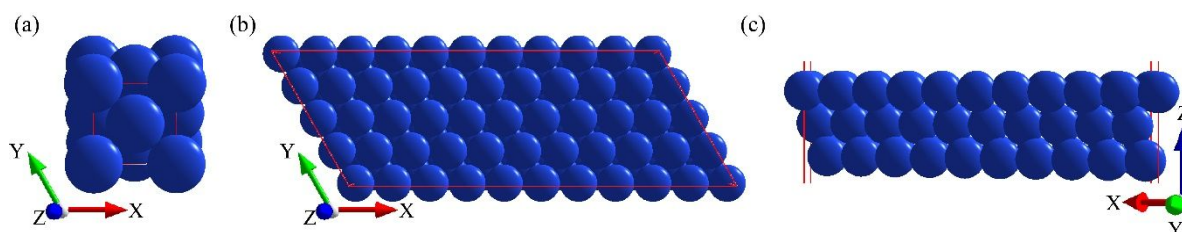


**Figure S2.** (a) Geometric structure of bulk Cu as seen along Z-direction. Geometric structures of Cu (111) surface (5x3x1 supercell), as seen along (b) Z- and (c) Y-directions.

**Figure S3**

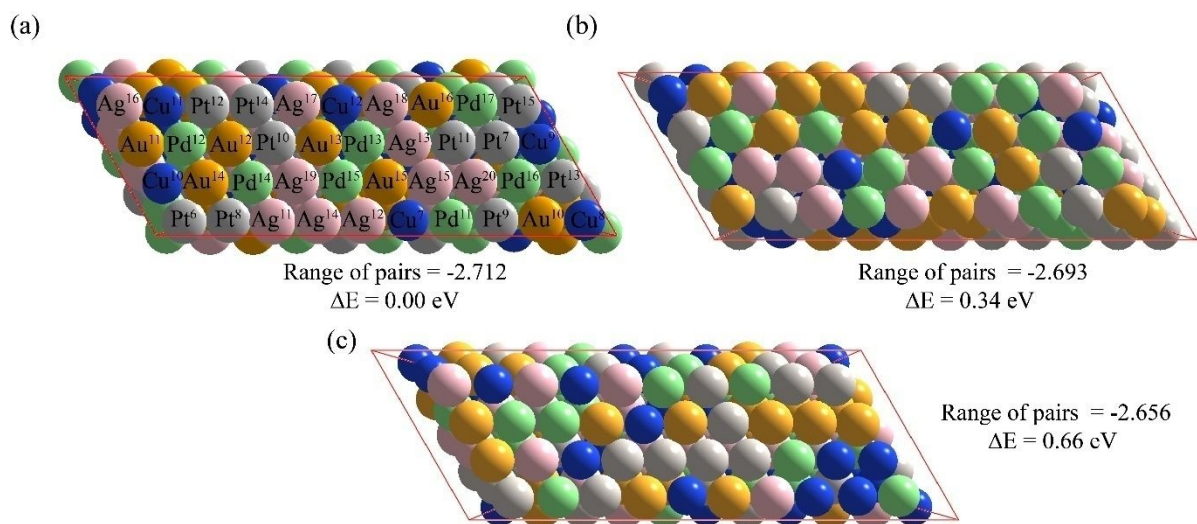


**Figure S3.** Optimized structures of SQS of AuAgPtPdCu HEA for (a) configuration-1, (b) configuration-2, and (c) configuration-3, along with the range of pairs and their relative energies. Atoms in the topmost layer have also been marked in (a), which is utilized for further calculations.

**Figure S4**

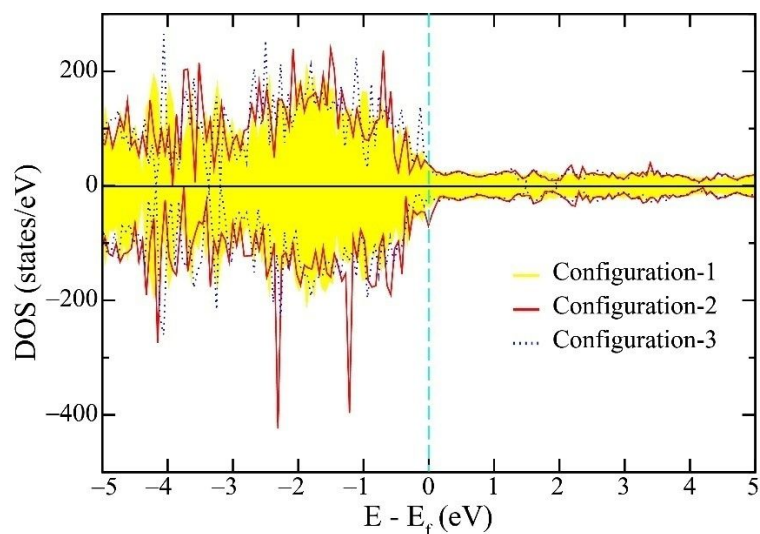
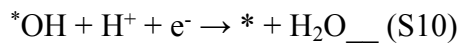
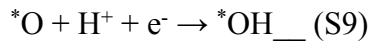
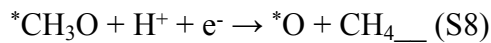
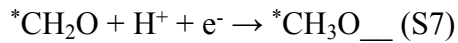
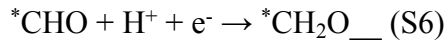
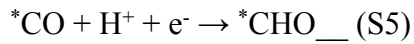
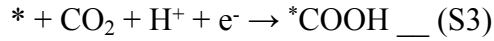


**Figure S4.** DOS of all three configurations of SQS of AuAgPtPdCu HEA, shown in Figure S3. The Fermi level is shown by cyan-dashed lines.

The eight elementary steps involved in CO<sub>2</sub>RR are:



Adsorption energies of the intermediates were calculated according to the given expressions:

$$\Delta E_{\text{COOH}}^{\text{ads}} = E_{\text{COOH}*} - E_* - (E_{\text{CO}_2} + 1/2E_{\text{H}_2}) \_ \_ \text{ (S11)}$$

$$\Delta E_{\text{CO}}^{\text{ads}} = E_{\text{CO}*} - E_* - (E_{\text{CO}}) \_ \_ \text{ (S12)}$$

$$\Delta E_{\text{CHO}}^{\text{ads}} = E_{\text{CHO}*} - E_* - (E_{\text{CO}} + 1/2E_{\text{H}_2}) \_ \_ \text{ (S13)}$$

$$\Delta E_{\text{CH}_2\text{O}}^{\text{ads}} = E_{\text{CH}_2\text{O}*} - E_* - (E_{\text{CO}_2} + E_{\text{H}_2}) \_ \_ \text{ (S14)}$$

$$\Delta E_{\text{CH}_3\text{O}}^{\text{ads}} = E_{\text{CH}_3\text{O}*} - E_* - (E_{\text{CO}_2} + 3/2E_{\text{H}_2}) \_ \_ \text{ (S15)}$$

$$\Delta E_{\text{O}}^{\text{ads}} = E_{\text{O}*} - E_* - (E_{\text{H}_2\text{O}} - E_{\text{H}_2}) \_ \_ \text{ (S16)}$$

$$\Delta E_{\text{OH}}^{\text{ads}} = E_{\text{HO}*} - E_* - (E_{\text{H}_2\text{O}} - 1/2E_{\text{H}_2}) \_ \_ \text{ (S17)}$$

\* represents pristine catalyst surface, and intermediates with \* superscript denotes the species being adsorbed on the catalyst surface.

**Figure S5**

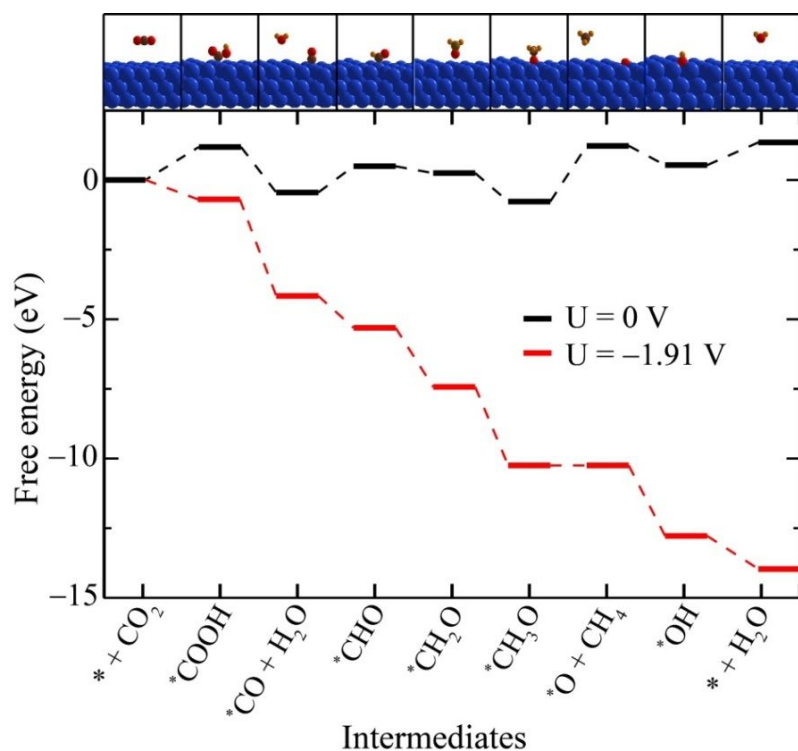


**Figure S5.** Free energy diagram of CO<sub>2</sub>RR on the pristine Cu (111) surface. Optimized structures of all the intermediates are shown in the inset.

**Figure S6**

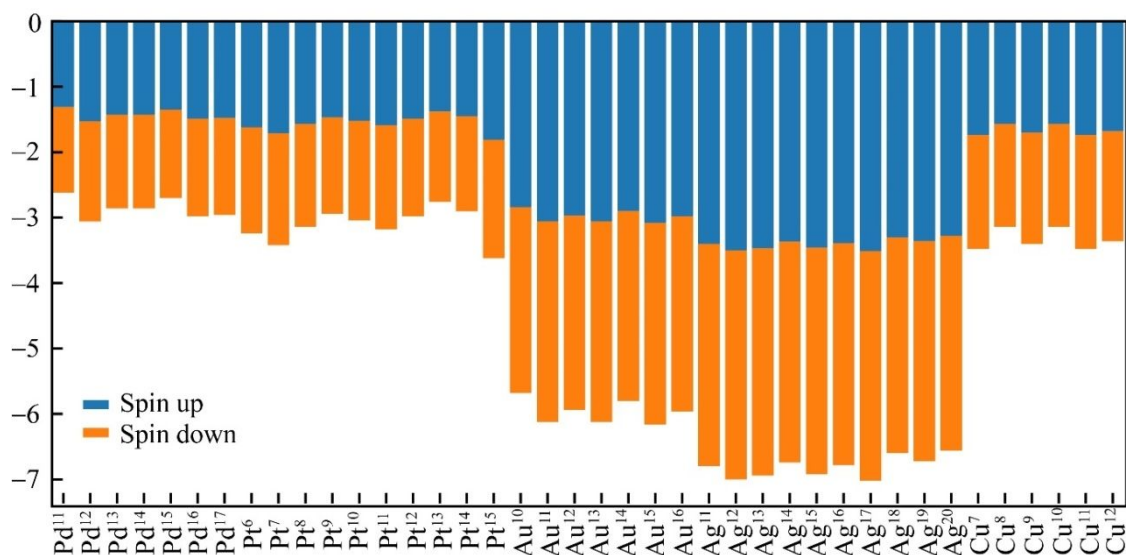


**Figure S6.** d-band center ( $E_{dBC}$ ) of all the atoms present on the topmost surface of AuAgPtPdCu HEA slab with respect to the Fermi level ( $E_F$ ).

**Figure S7**

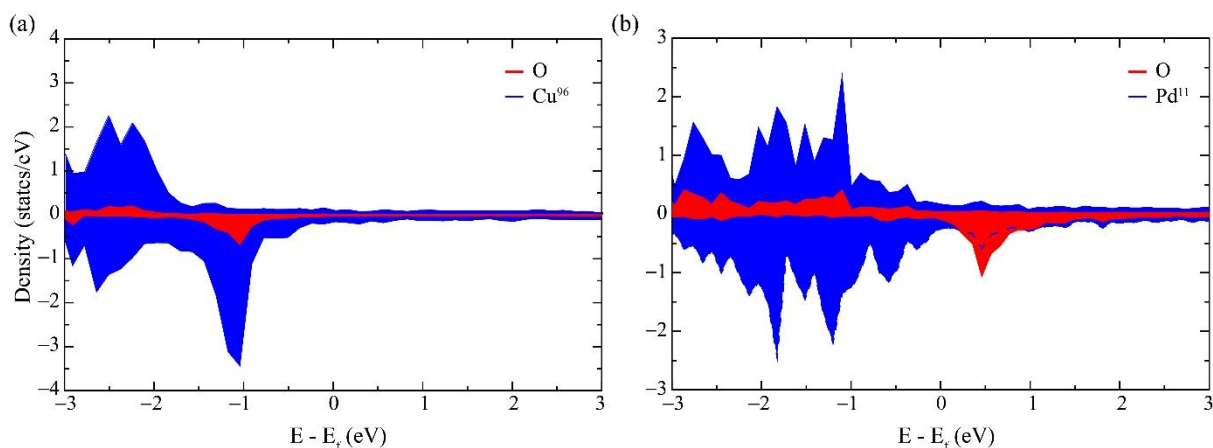


**Figure S7.** Partial density of states (PDOS) of O atom of  $^*OCH_3$  (red curve) adsorbate compared with that of (a)  $Cu^{96}$  (blue curve) on the Cu (111) surface and (b)  $Pd^{11}$  (blue curve) on the HEA surface. Both the metal atoms chosen are the catalytic sites on the two systems.

**Figure S8**

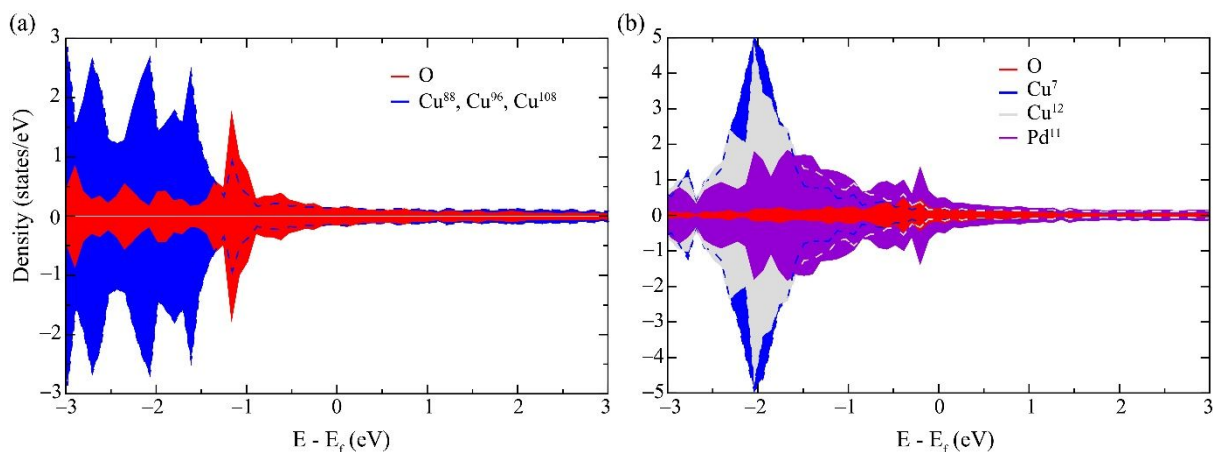


**Figure S8.** Partial density of states (PDOS) of O atom of  $^*O$  (red curve) adsorbate compared with that of (a)  $Cu^{88}$ ,  $Cu^{96}$ , and  $Cu^{108}$  (blue curve) on the Cu (111) surface and (b)  $Cu^7$  (blue curve),  $Cu^{12}$  (grey curve), and  $Pd^{11}$  (violet curve) on the HEA surface. All the metal atoms chosen are catalytic sites on the two systems.

**Figure S9**

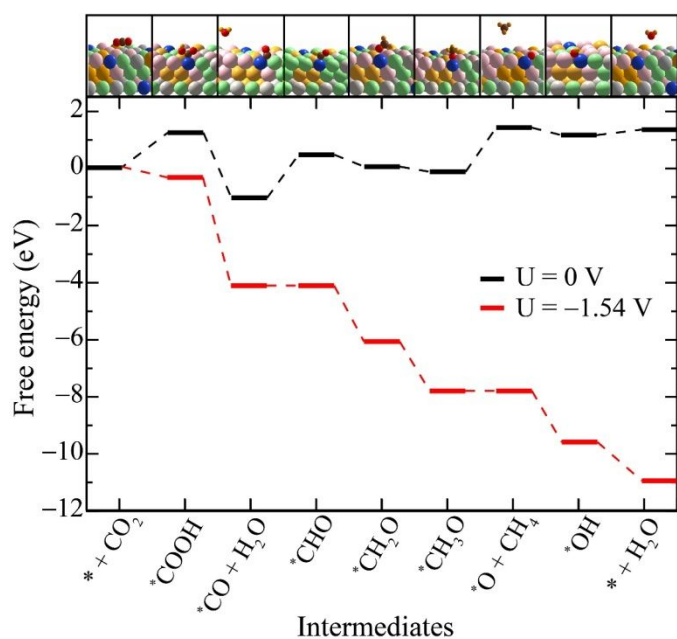


**Figure S9.** Free energy diagram of CO<sub>2</sub>RR on Cu-7 active site of the HEA surface. Optimized structures of all the intermediates are shown in the inset.

**Figure S10**

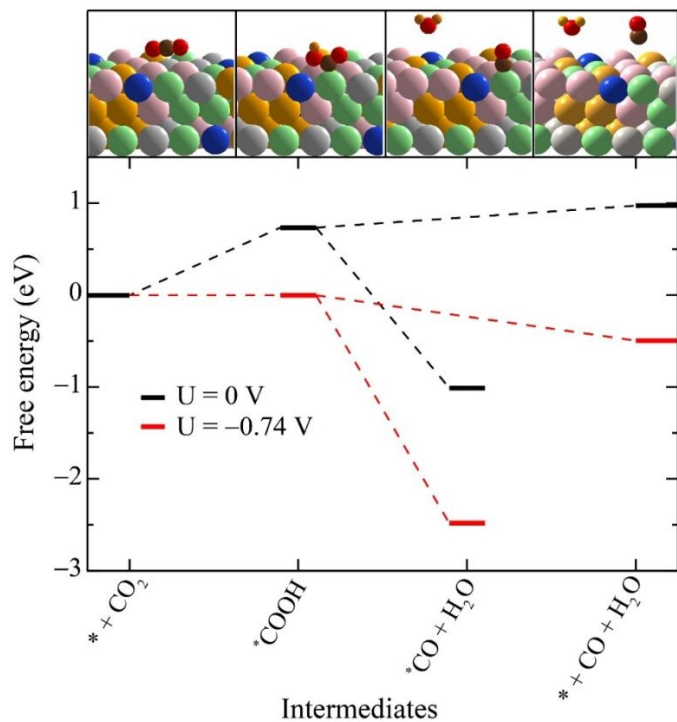


**Figure S10.** Free energy diagram for CO evolution on Pd-11 active site of the HEA surface. Optimized structures of all the intermediates are shown in the inset.

**Figure S11**

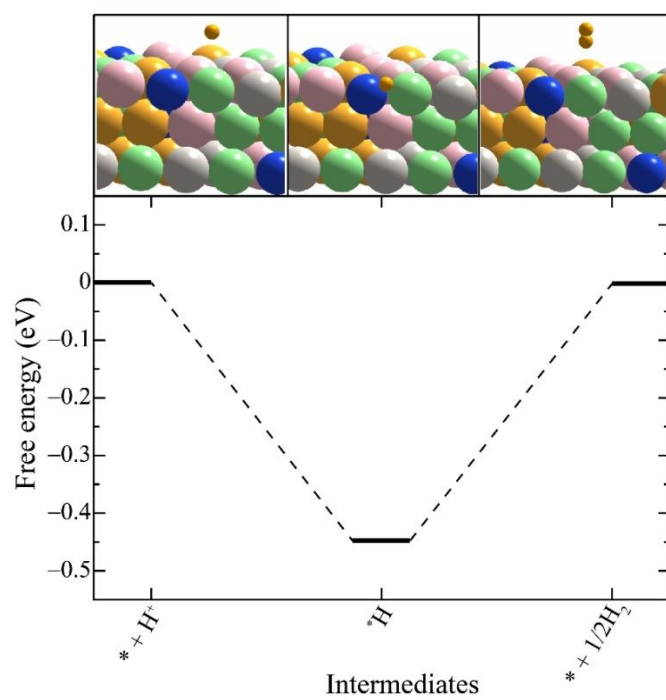


**Figure S11.** Free energy diagram for H<sub>2</sub> evolution on Pd-11 active site of the HEA surface. Optimized structures of all the intermediates are shown in the inset.

**Table S1.** Comparative catalytic activities of HEA with other reported nanocatalysts.

S.No	Electrocatalyst	Electrolyte	Applied potentials	Products (FE%)	Total
1	Polycrystalline Cu <sup>8</sup>	0.1 M KHCO <sub>3</sub>	-1.05 V <sub>RHE</sub>	CH <sub>4</sub> (24.4); C <sub>2</sub> H <sub>4</sub> (26.0); CO (1.1); H <sub>2</sub> (23.0); C <sub>2</sub> H <sub>5</sub> OH (9.8); HCOOH (2.1)	91.2%
2	Cu mesocrystals <sup>9</sup>	0.1 M KHCO <sub>3</sub>	-0.99 V <sub>RHE</sub>	CH <sub>4</sub> (1.47); C <sub>2</sub> H <sub>4</sub> (27.2); CO (0.55); H <sub>2</sub> (66.5); HCOOH (4.3)	100.1%
3	Cu nanoparticles <sup>10</sup>	0.1 M KClO <sub>4</sub>	-1.1 V <sub>RHE</sub>	CH <sub>4</sub> (1);C <sub>2</sub> H <sub>4</sub> (36); CO (34),	72.0%
4	Cu nano particles <sup>11</sup>	0.1 M NaHCO <sub>3</sub>	-1.25 V <sub>RHE</sub>	CH <sub>4</sub> (80%); H <sub>2</sub> (13%)	93.0%
5	Cu nanowires <sup>12</sup>	0.1 M KHCO <sub>3</sub>	-0.795 V <sub>RHE</sub>	CO (2.4); C <sub>2</sub> H <sub>4</sub> (7.2); C <sub>2</sub> H <sub>6</sub> (8.6);H <sub>2</sub> (56%); HCOOH (9.6); CH <sub>3</sub> CH <sub>2</sub> OH (10.8)	94.6%
6	Cu nanoflower <sup>13</sup>	0.1 M KHCO <sub>3</sub>	-1.6 V <sub>RHE</sub>	CH <sub>4</sub> (5); C <sub>2</sub> H <sub>4</sub> (10); H <sub>2</sub> (29); HCOOH (49)	94.0%
7	Cu nano (10 nm) <sup>14</sup>	0.1 M KHCO <sub>3</sub>	-1.1 V <sub>RHE</sub>	CH <sub>4</sub> (10); C <sub>2</sub> H <sub>4</sub> (4); CO (22); H <sub>2</sub> (64)	100.0%
8	Ag nano (5 nm) <sup>15</sup>	0.5 M KHCO <sub>3</sub>	-0.75 V <sub>RHE</sub>	CO (79.2)	79.20%
9	Au nano (3.2 nm) <sup>16</sup>	0.1 M KHCO <sub>3</sub>	-1.2 V <sub>RHE</sub>	CO (20); H <sub>2</sub> (80)	100.0%
10	Pd nano (3.7 nm) <sup>17</sup>	0.1 M KHCO <sub>3</sub>	-0.89 V <sub>RHE</sub>	CO (91.2)	91.2%
11	<b>AuAgCuPdPt</b>	<b>0.5 M K<sub>2</sub>SO<sub>4</sub></b>	<b>-0.9 V<sub>Ag/AgCl</sub></b> (-0.3V <sub>RHE</sub> )	<b>CH<sub>4</sub> (38.2); C<sub>2</sub>H<sub>4</sub> (29.5);CO (4.9);H<sub>2</sub> (27.5)</b>	<b>100.1%</b>

## REFERENCES

- (1) Kumar, N.; Tiwary, C. S.; Biswas, K. Preparation of Nanocrystalline High-entropy Alloys via Cryomilling of Cast Ingots. *J. Mater. Sci.* **2018**, *53*, 13411–13423.
- (2) Kresse, G.; Hafner, J. Ab initio Molecular Dynamics for Liquid Metals. *Phys. Rev. B* **1993**, *47*, 558
- (3) Perdew, J. P.; Burke, K.; Ernzerhof, M. Generalized Gradient Approximation Made Simple. *Phys Rev Lett.* **1996**, *77*, 3865-3868.
- (4) Zunger, A.; Wei, S.-H.; Ferreira, L. G.; Bernard, J. E. Special Quasirandom Structures, *Phys. Rev. Lett.* **1990**, *65*, 353-356.
- (5) van de Walle A, *et al.* Efficient stochastic generation of special quasirandom structures. *Calphad* **2013**, *42*, 13-18.

- (6) Hass, K. C.; Davis, L. C.; Zunger, A. Electronic Structure of Random  $\text{Al}_{0.5}\text{Ga}_{0.5}\text{As}$  Alloys: Test of the "Special-Quasirandom-Structures" Description. *Phys. Rev. B* **1990**, *42*, 3757-3760.
- (7) Jiang, C.; Stanek, C. R.; Sickafus, K. E.; Uberuaga, B. P. First-Principles Prediction of Disordering Tendencies in Pyrochlore Oxides. *Phys. Rev. B* **2009**, *79*, 104203-104208.
- (8) Kuhl, K. P.; Cave, E. R.; Abram, D. N.; Jaramillo, T. F. New Insights Into the Electrochemical Reduction of Carbon Dioxide on Metallic Copper Surfaces. *Energy Environ. Sci.* **2012**, *5*, 7050-7059.
- (9) Chen, C. S.; Handoko, A. D.; Wan, J. H.; Ma, L.; Ren, D.; Yeo, B. S. Stable and Selective Electrochemical Reduction of Carbon Dioxide to Ethylene on Copper Mesocrystals. *Catal. Sci. Technol.* **2015**, *5*, 161-168.
- (10) Tang, W.; Peterson, A. A.; Varela, A. S.; Jovanov, Z. P.; Bech, L.; Durand, W. J.; Dahl, S.; Norskov, J. K.; Chorkendorff, I. The Importance of Surface Morphology in Controlling the Selectivity of Polycrystalline Copper for  $\text{CO}_2$  Electroreduction. *Phys. Chem. Chem. Phys.* **2012**, *14*, 76-81.
- (11) Manthiram, K.; Beberwyck, B. J.; Alivisatos, A. P. Enhanced Electrochemical Methanation of Carbon Dioxide with a Dispersible Nanoscale Copper Catalyst. *J. Am. Chem. Soc.* **2014**, *136*, 13319-13325.
- (12) Raciti, D.; Livi, K. J.; Wang, C. Highly Dense Cu nanowires for Low-overpotential  $\text{CO}_2$  Reduction. *Nano Lett.* **2015**, *15*, 6829-6835.
- (13) Xie, J.-F.; Huang, Y.-X.; Li, W.-W.; Song, X.-N.; Xiong, L.; Y, H.-Q. Efficient Electrochemical  $\text{CO}_2$  Reduction on a Unique Chrysanthemum-like Cu Nanoflower Electrode and Direct Observation of Carbon Deposit. *Electrochim. Acta* **2014**, *139*, 137-144.
- (14) Reske, R.; Mistry, H.; Behafarid, F.; Cuenya, B. R.; Strasser, P. Particle Size Effects in the Catalytic Electroreduction of  $\text{CO}_2$  on Cu Nanoparticles. *J. Am. Chem. Soc.* **2014**, *136*, 6978-6989.
- (15) Kim, C.; Jeon, H. S.; Eom, T.; Jee, M. S.; Kim, H.; Friend, C. M.; Min, B. K.; Hwang, Y. J. Achieving Selective and Efficient Electrocatalytic Activity for  $\text{CO}_2$  Reduction Using Immobilized Silver Nanoparticles. *J. Am. Chem. Soc.* **2015**, *137*, 13844-13850.
- (16) Mistry, H.; Reske, R.; Zeng, Z.; Zhao, Z. J.; Greeley, J.; Strasser, P.; Cuenya, B. R. Exceptional Size-Dependent Activity Enhancement in the Electroreduction of  $\text{CO}_2$  over Au Nanoparticles. *J. Am. Chem. Soc.* **2014**, *136*, 16473-16476.
- (17) Gao, D.; Zhou, H.; Wang, J.; Miao, S.; Yang, F.; Wang, G.; Wang, J.; Bao, X. Size-Dependent Electrocatalytic Reduction of  $\text{CO}_2$  over Pd Nanoparticles. *J. Am. Chem. Soc.* **2015**, *137*, 4288-4291.

\*\*\*\*\*